2. MATERIALS AND METHODOLOGY OF EXPERIMENTAL RESEARCH

According to the thermodynamic assessment of predicting the possibility of the course of the thermochemical process [1, 2], all investigated intermetallic formation reactions were divided into two groups based on the ratio of the adiabatic combustion temperature and the melting temperature of the resulting product. In the first group, a system is selected in which the adiabatic combustion temperature is lower than the melting temperature of the resulting compound – the *Ti-Al* system ($T_{ad} < T_{melt}$). From the second group, a system was selected for which the adiabatic combustion temperature is equal to or exceeds the melting temperature of the product formed – the *Ni-Al* system ($T_{ad} \geq T_{melt}$). Therefore, intermetallic alloys became the object of research, such as *Ni-Al* and *Ti-Al*, which belong to two different systems.

2.1. Objects, materials and equipment

It is known that in the technology of thermochemical pressing, the material used is an exothermic mixture of powder components in a bulk or compressed state. When preparing reaction mixtures of different compositions in the studied *Ti-Al-ЛЕ* and *Ni-Al-ЛЕ* systems, powders of the following brands were used: aluminum powder of the ASD-4 brand – a source of aluminum in the alloy; PTEM-1 grade electrolytic titanium powder – a source of titanium in the alloy; nickel electrolytic powder of the PNE-1 brand – a source of nickel in the alloy; PChA brand chromium powder is a source of chromium in the alloy; Cobalt powder brand PK1 – a source of cobalt in the alloy; MPCh molybdenum powder is a source of molybdenum in the alloy; niobium powder grade Nb-1 is a source of niobium in the alloy.

The characteristics of the initial components and histograms of particle size distribution are presented in **Table 2.1** and **Fig. 2.1**.

Table 2.1 Characteristics of the initial components

Material	**Chemical composition, %**	**Average particle size, mm**
ASD–4	*Al* – not smaller than 99.7, *Fe* – up to 0.2, *Si* – up to 0.2, other – up to 0.3	0.00348
PTEM –1	*Ti* – not smaller than 99.7, *Fe* – up to 0.08, *Cl* – up to 0.05, *N* – up to 0.03, *C* – up to 0.03, *Si* – up to 0.04	0.00223
PNE –1	*Ni* – not smaller than 99.5, *Fe* – up to 0.01, *C* – up to 0.02, *Si* – up to 0.03, *Co* – up to 0.2, *Cu* – up to 0.06, *O* – до 0.1	0.00878
PChA	*Cr* – not smaller than 97.5, *Si* – up to 0.5, *Al* – up to 1.5, *Fe* – up to 1.5, C – up to 0.04	0.00125
PK1	*Co* – not smaller than 99.35, *Fe* – up to 0.2, *Si* – up to 0.02, *Ni* – up to 0.4, *C* – up to 0.02, *Cu* – up to 0.04	0.00886
MPCh	*Mo* – not smaller than 99.7, *W* – up to 0.2, *O* – up to 0.25, *C* – up to 0.009, *Fe* – up to 0.005	0.00304
Nb–1	*Nb* – not smaller than 99.7, *N* – up to 0.01, *O* – up to 0.01, *C* – up to 0.01, *Ta* – up to 0.1, *Fe* – up to 0.005, *Ti* – up to 0.005, *W+Mo* – up to 0.01	0.04909

Before mixing, all initial powders were dried to remove moisture in a drying cabinet at a temperature not lower than 90 °C. The drying time of the powders was 24 hours. Dosing of the components of the charge was carried out on technical scales of the ВЕСТУ В1505 brand with an accuracy of 0.01 g.

Cylindrical samples with a diameter of 11.3 and 25 mm and a height of 16…20 mm were formed from the charge by the method of double-sided pressing in a collapsible steel mold (GOST 25280-90). The volumetric thermal explosion mode is observed only for high-density samples: $\Delta = 0.7…0.8$ for the *Ni-Al* system and $\Delta = 0.55…0.8$ for *Ti–Al*. A decrease in density in the first system leads to a frontal combustion mode and the absence of an intense exothermic reaction in the second [2, 3].

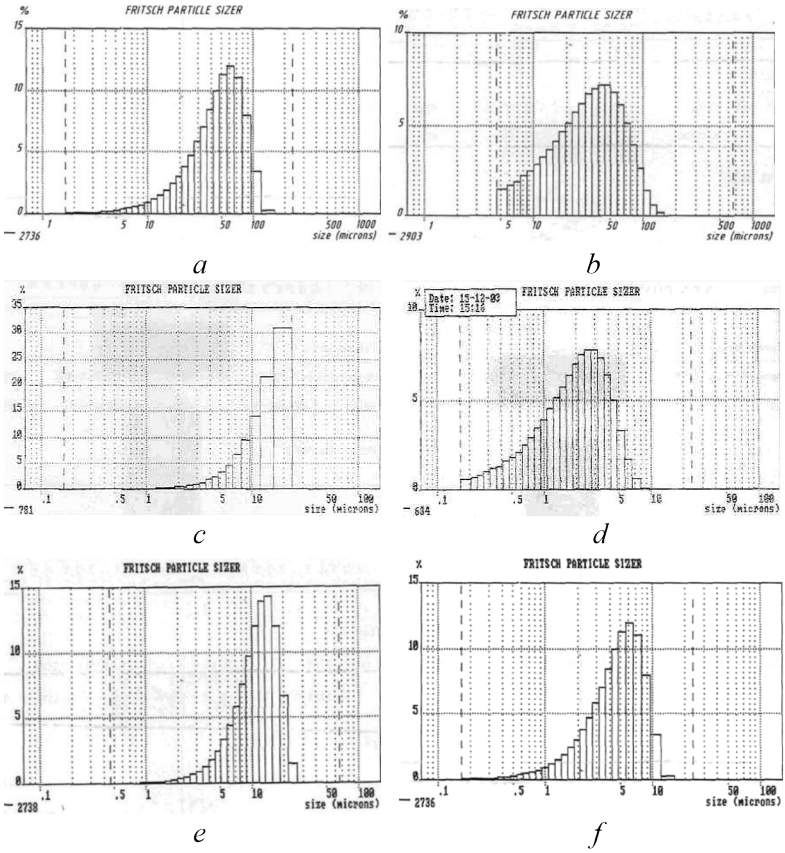

a – aluminum; b – titanium; c – nickel; d – chromium; e – cobalt; f – molybdenum

Fig. 2.1. Particle size distribution

Production of intermetallic alloys under the conditions of thermochemical pressing was carried out at the installation, the schematic diagram of which is shown on **Fig. 2.3**.

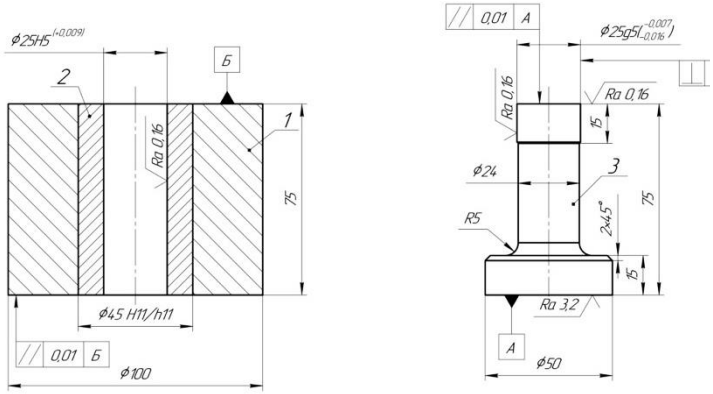

a

b

a – mold diameter 25 мм, б – natural models

Fig. 2.2. Molds for pressing cylindrical samples

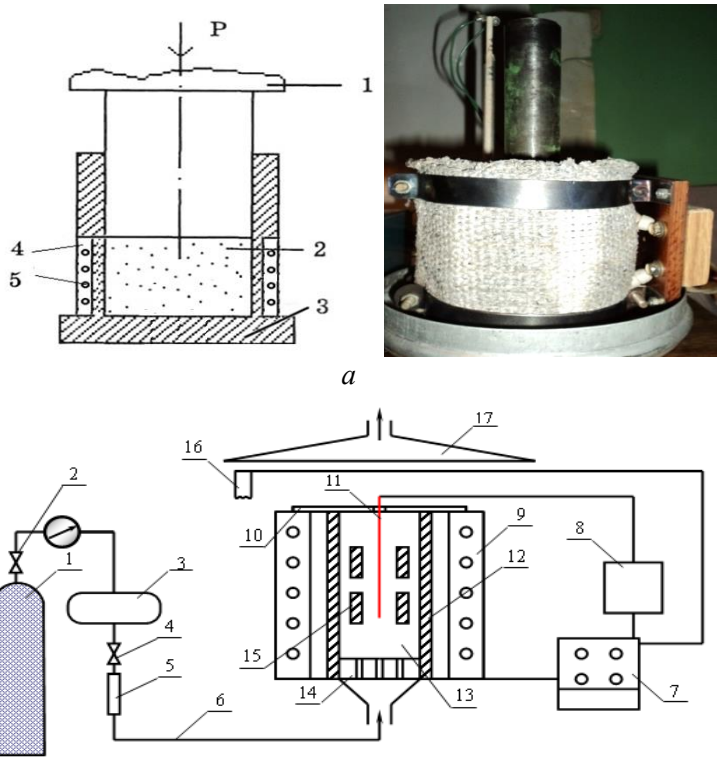

a – a reaction mold, b – a complete scheme of the installation:
1 – gas cylinder; 2 – reducer; 3 – receiver; 4 – valve; 5 – flow meter; 6 – gas main;
7 – power supply unit; 8 – temperature controller "Micro 600"; 9 – electric stove;
10 – reactor cover; 11 – thermocouple; 12 – reactor; 13 – reaction mixture;
14 – porous gratings; 15 – samples; 16 – electrospiral; 17 – gas utilization system

Fig. 2.3. Schematic diagram of the installation for obtaining intermetallic alloys under thermochemical pressing conditions

The installation consists of the following main functional systems: reaction equipment, gas supply system, control and regulation system technological parameters, gas utilization systems. The equipment consists of a reactor 12, on the bottom of which porous grids 14 are installed, which stabilizes the level of the reaction mixture 13. For the process of obtaining intermetallic alloys, which is carried out under the conditions of thermochemical pressing, reagents of the classification "h" and "chda" were used. The bottom of the reactor is a cover with an inlet pipe mounted in the center, which connects to the gas line 6. To reduce heat losses and reliably fix the thermocouple, the reactor is closed from above with an asbestos cover 10. The reactor was heated in a shaft-type furnace 9. When the process was implemented in the combustion mode, the installation equipped with an electric coil of the ignition device 16.

The gas supply system consists of cylinder 1 with inert gas (argon), which enters reactor 12 through reducer 2, receiver 3, valves 4, flowmeters 5 and gas line 6. Receiver 3 can ensure the constancy of the gas supply rate when conducting processes at several reactors. The system of control and regulation of technological parameters: the regulation of the rate of heating of the reaction mixture is carried out through the power supply unit 7, which controls the power of the furnace 9; temperature measurement was carried out by the "Micro600" temperature controller 8 with a tungsten-rhenium thermocouple (BP-5) with an accuracy of ± 5 °C 11; the inert gas supply rate was measured using valve 4, which is connected through the gas line to the flow meter 5. The processes were carried out using local exhaust ventilation 17. For thermochemical pressing of the blanks, a hydraulic press was used, developing a force of up to 1.25 MN. The technological scheme for the preparation of the charge included dosing, mixing, filling the mold, cold double-sided pressing, thermochemical pressing and heat treatment.

2.2. Methodology of the experiment

2.2.1. Testing and control of materials

Kinetics was studied using microstructural analysis of the obtained samples. The research was conducted on samples with dimensions of 30 × 20, 30 × 30, 30 × 40 mm. Determinations were made on cross-sections on a Neophot-21 microscope.

Metallographic analysis. The microstructure was studied from transverse sections on a Neophot-21 microscope at a magnification of × 50–500.

During the production of cross sections, in order to prevent the edges from collapsing, the samples were clamped in steel clamps. After grinding on emery paper, polishing was performed with diamond pastes with a successive decrease in the grain size to 0/1 μm. The final polishing was done on the dress in the presence of an aqueous chromium oxide emulsion.

X-ray structural analysis. X-ray units "DRON-3" and "DRON-2" in *CuK*α radiation with the use of a nickel filter, working together with the computing complex according to the "ARFA" program, were used to study the phase composition of coatings and spent charge. Radiography was performed in the automatic mode of recording diffraction lines on a chart tape with a counter movement speed of 1 deg/min in the range of angles 2θ = 15 – 163o.

Thermogravimetry. Thermogravimetric studies of the compound were performed on a TAG24 S24 SETARAM derivatograph in air with a heating rate of 2.5 degrees/min from 27 to 202 °C. The suspension of the substance did not exceed 400 mg. The error in determining the temperature of the sample during thermogravimetric experiments was less than 3°.

Heat resistance. Heat resistance tests were carried out on cylindrical samples with a diameter of 10.0 ± 0.2 mm and a height

of 20.0 ± 0.5 mm in air in the temperature range of 800…1700 °C, followed by weighing on analytical balances. Based on the possibilities available in the department's laboratory, the thermal equipment of the electric furnace SNOL-1,6.2,0.0,8/9-M1 was used in the work.

Porosity. Porosity was determined by the formula:

$$П = \left[1 - \left(\frac{M}{V}\right)\left(\frac{\%A}{\rho_A} + \frac{\%B}{\rho_B}\right)\right] 100\%, \qquad (2.1)$$

where M – mass of the workpiece (g), determined by weighing on electronic scales with an accuracy of 0.01 g;

V – the volume of the cylindrical workpiece (mm^3), determined by measuring the diameter and height with a caliper;

$\%A$ $\%B$ – percentage ratio by mass of metals in the charge;

ρ_A, ρ_B – theoretical density of metals (g/mm^3).

Durability test. The mechanical strength of the obtained samples was determined using a UG-20 machine. Compression and bending tests were performed respectively. The compression test specimens were 20 mm in diameter and 20 mm in height. The bending test specimens had a diameter of 40 mm and a length of 340 mm with a distance between the centers of the supports of 300 mm.

Wear resistance test. Tests for wear resistance were carried out during friction on the SMT-1 installation. To create an abrasive-oil environment, an abrasive material prepared from quartz sand at a concentration of 3 ± 0.5 % by mass was added to the oil bath of the friction machine.

2.2.2. Planning and processing of experiment results

Different systems were used in the study to determine the effect of heat resistance and hardness of cements on pressing force, *TiC* content and alloying components (*Ni, Mo, W*): *Ti-C-Ni-Al, Ti-C-Ni-Al, Ti-C-Ni-Al*.

Drawing up an experiment plan. When drawing up the plan of the planned factorial experiment, it is necessary to ensure that there are no repetitions. To avoid repetition of experiments, let's use the principle (**Table 2.2**).

Table 2.2 The matrix of the planned factorial experiment

Plan	Experiment number	X_0	X_1	X_2	X_3
2^2	1	+	+	+	+
	2	+	–	+	+
	3	+	+	–	+
	4	+	–	–	+
2^3	5	+	+	+	–
	6	+	–	+	–
	7	+	+	–	–
	8	+	–	–	–

The factor marked "X_0" – this is what we call the dummy variable – we enter it to calculate the free term of the desired model – the"b_0". coefficient

After compiling the table, we check the correctness of its filling. The replica symmetry condition requires that each column contains an equal number of minuses and pluses. The condition is fulfilled.

Implementation of the experiment plan. To determine the error of the experiment, the experiments should be duplicated. More often, not all experiments are duplicated, but only experiments at the basic level. In this case, the variance of the S_y experiment is calculated according to the formula:

$$S_y^2 = \sum_{i=1}^{n} \frac{(Yoi - Yo)^2}{f_1}, \qquad (2.2)$$

where n – the number of takes at the main level;

i – nuber of the take;

Y_{oi} – the value of the optimization parameter in the i take;

Y_o – the arithmetic mean of the results of all takes;

$f_1 = n - 1$.

Construction of a mathematical model. After the implementation of all experiments of the planning matrix, a mathematical model of the process under study is built based on their results. For this we calculate the regression coefficients of the equation using the formula:

$$b_j = \sum_{j=1}^{n} \frac{X_{jn} \cdot Y_n}{N}, \tag{2.3}$$

where b_j – value of the j regression coefficient;

X_{jn} – value of the j factor in n experiment in coded form Y_n – value of the optimization parameter in n experiment;

N – number of trials in the planning matrix.

As a result, a model is obtained, which has the following form:

$$Y = b_0 + b_1 X_1 + b_2 X_2 + b_3 X_3 + \ldots + b_j X_j. \tag{2.4}$$

Statistical analysis of the model. The purpose of the analysis is to check the suitability of the model for its use in describing the object under study.

The analysis consists of two stages. At the first stage, we check the statistical significance of the regression coefficients. In statistics, it is customary to check the significance of regression coefficients using the Student's test. For this, we calculate the confidence interval of the coefficients:

$$\Delta b_i = t_{\alpha, f_1} \cdot S_{bi}, \tag{2.5}$$

where S_{bi} – root mean square error in determining the regression coefficients:

$$S_{bi} = \sqrt{\frac{S_y^2}{N}}, \tag{2.6}$$

$t_{D,f1}$ – value of Student's criterion, which is selected depending on the level of significance D and the number of degrees of freedom when determining the variance of the experiment f_1.

We compare the values of the regression coefficients with i–those that are less than the confidence interval in absolute value and are excluded from the equation.

At the second stage, the finally obtained equation is checked for adequacy, that is, its suitability for describing the research object.

Therefore, we check the adequacy of the obtained models as a whole. To do this, we substitute the value of "X_i" in the coded form, which we take from Table 2.2, into the resulting equation sequentially for all experiments.

To determine the dispersion of inadequacy, we compile a calculation table. The table is compiled based on the algorithm for checking the obtained equation for adequacy, that is, its suitability for describing the object of research. The check sequence is as follows:

1. According to the contents of the model, the values of the optimization parameter are calculated through all traces of the planning matrix (y_{calc}). To do this, we substitute the values of the factors in coded form into the equation.

2. Using the formula, we obtain an estimate of the dispersion of inadequacy:

$$S^2_{inad} = \frac{\sum_{n=1}^{N}\left(y_n^{exper} - y_n^{calc}\right)^2}{f_2}, \qquad (2.7)$$

where $f_2 = N - K'$, K' – number of model coefficients, including b_0.

3. The calculated value of the Fisher criterion is determined and compared with the tabular one, which is selected from the table in work [32] depending on the level of significance D and the number of degrees of freedom f_1, f_2.

$$F^{calc}_{f1,f2} = \frac{S^2_{inad}}{S^2_y}. \qquad (2.8)$$

Interpretation of results. The obtained adequate model allows to calculate the value of the optimization parameter for any point of the studied factor space.

In addition, the obtained dependence can be presented graphically in the form of the influence of individual factors on the optimization parameter. At the same time, the dependence $y = f(x_i)$ is usually built

on the condition that all other factors are fixed at a constant level. Then we substitute the value of factor X_2 and X_3 in coded form (with the sign "–") into this equation.

Then, in the transformed (simplified) equation, we successively substitute the value of factor X_1 at the lower, main and upper levels, i.e. −1; 0; +1 and we get the desired graph [32].

2.3. Preparatory stage of thermochemical pressing

The pressing process consists of several stages. The first stage is preparatory, where a batch briquette was made from a mixture of initial powders in a separate mold. The pressing pressure range was 70…100 MPa, the loading speed was manually controlled and maintained in the range of 0.1…0.5 MPa/s. In order to more evenly distribute the pressing pressure over the volume of the workpiece, a holding time of 20 seconds was carried out.

The compressibility of non-ferrous metal powders is determined to a certain extent by the manufacturing methods. It is known that depending on the fraction of the powder, its chemical composition changes. Large fractions of the powder, as a rule, have fewer harmful impurities due to their low absorption capacity due to the small specific surface area. The physical properties of powders are determined by the size of the particles, their shape, microhardness, specific surface area, pycnometric density, and the degree of imperfection of the crystal lattice of the powder particles. The size and shape of the particles depend on the method of preparation of powders, so each method of obtaining powders is characterized by a specific shape of particles. However, in some cases, powders of the same origin have different particle shapes, and the particle sizes of the powder of the same origin, as a rule, vary within quite wide limits.

Technological properties are characterized by bulk density, fluidity of the powder and compressibility of the powder. These characteristics

functionally derive from the properties listed above. Determination of technological properties is extremely necessary, because knowledge of them determines the choice of appropriate equipment and tools. The technological properties of powders of various metals are presented in the works [33, 34].

Table 2.3 shows the technological properties of titanium powders obtained by various methods.

Table 2.3. Technological properties of titanium powders

Powder type	I	II	III
Average particle size, μm	180	56.6	18.4
Bulk density, $t/m^3 \cdot 10^3$	1.40…1.53	1.50…1.55	1.16…1.18
Fluidity, $kg/s \cdot 10^4$	3.6	3.0…3.2	2.6…2.8
Specific surface area, m^2/kg	70…90	100…110	120…125
Hardness, BHN	90…120	130…150	125…130
I – electrolytic, II – hydride, III – calcium hydride			

Bulk density to a certain extent determines the technology of pressing and sintering. Knowing the value of the bulk density is very important when designing molds, as well as in the practice of cold pressing, when the dosage of the charge is carried out by the usual method. The constancy of the dimensions and density of pressed briquettes in this case is determined by the invariance of the bulk density of the charge. The lower the bulk density of the charge, the greater the amount of powder required for the manufacture of products of the given size and density, which leads to an increase in the dimensions of the container and punch, causing additional difficulties in the manufacture of equipment and operation of the equipment. Fluctuations in bulk density affect the results of sintering and the physical properties of the finished product. Shrinkage after sintering

decreases with increasing bulk density, which in turn depends on the particle size composition of the powders.

The graphical method provides certain advantages for determining the parameters of pressed briquettes.

Fig. 2.4 shows a nomogram for determining the geometric dimensions of a titanium briquette, its mass, pressing force, amount of powder filling depending on the ratio of the height of the briquette *H* to its diameter *D*.

The nomogram consists of four quadrants: I shows the dependence of the backfill mass G on the *H/D* ratio at *D* = 8, 13, 16, 25 mm and the

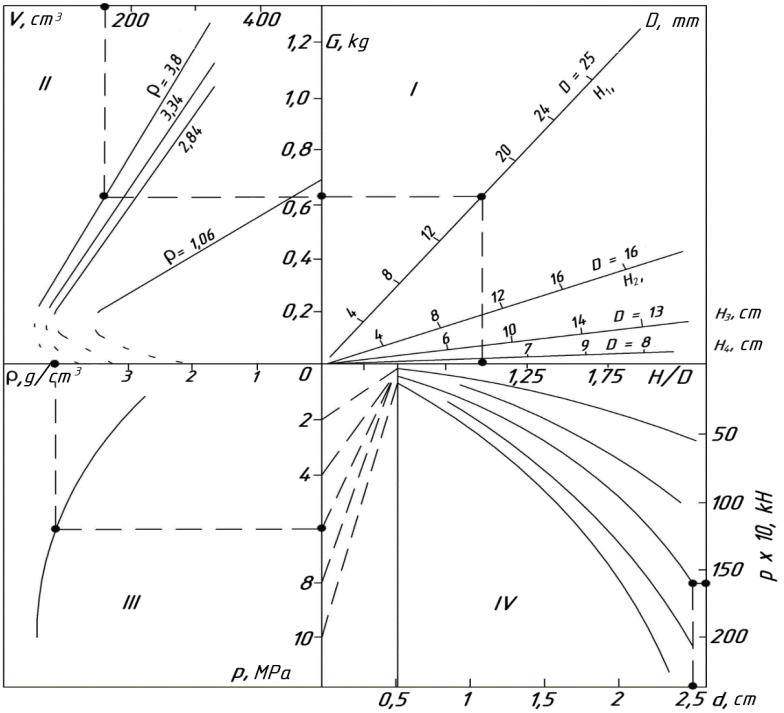

Fig. 2.4. Nomogram for determining the parameters of cold pressing of titanium powder briquettes

dependence of the backfill height H of the container on the briquette mass G; in II – the dependence of the volume of the briquette V on the mass of the briquette G and its density ρ, in III – the experimental dependence between the specific pressing force p and the density of the briquette ρ, in IV – the dependence of the pressing force P on the diameter of the briquette d and the specific pressure p. All 4 quadrants are interconnected with the resulting density of briquettes $\rho_{depend} = 70$, 80, 90 %. The III and IV quadrants of the nomogram have an independent value and are intended to determine the force parameters of pressing at a given density, and vice versa.

If you determine the briquette pressing parameters $D = 25$ mm at $H/D = 1$, density $\rho = 3.8$ t/m^3, then it is necessary to draw a dotted line with an arrow parallel to the ordinate axis in the first quadrant from the point $H/D = 1$ to the intersection with by the corresponding straight line $D = 25$ mm. The point of intersection gives the height of the filling of the container $H_1 = 16.96$ cm. Having drawn a line parallel to the abscissa axis from this point to the intersection with the ordinate axis, we obtain the value of the mass $G = 0.615$ kg and continue the line to the intersection with the density line $\rho = 3.8$ t/m^3. The point of intersection, projected on a scale ruler of volumes, gives the value of the volume of the finished briquette (V = 1,5–10^{-4} m^3). Descending along the density line, we pass to the III quadrant, where we get the point of intersection with the experimental curve $\rho = f(p)$. The density equal to $\rho = 3.8$ t/m^3 corresponds to the pressure $\rho = 600$ MPa. Next, in the IV quadrant, from the point corresponding to $d = 25$ mm, we draw a straight line parallel to the ordinate axis to the intersection with the force curve corresponding to $p = 600$ MPa, and we obtain a point corresponding to the pressing force $P = 1.56$ MN.

One of the most important regularities of the process of pressing metal powders is the quantitative dependence of the density of the powder body on the pressure exerted from the outside. The first and most complete developments on this issue belong to M. Y. Balshin, who proposed equations, of which the most well-founded:

$$\log p = -m \log \beta + \log p_{max}, \tag{2.9}$$

where p – pressing pressure;

p_{max} – pressing pressure, which ensures obtaining pressing of the theoretical density;

m – constants that take into account the nature of the pressed material and are called the pressing factor and index, respectively;

β – relative pressing volume.

The monograph [1] proposed an equation:

$$p_k = \frac{\left(p_k'\right)_0}{1 - 2v_k\sqrt{\alpha}}, \tag{2.10}$$

where $\left(p_k'\right)_0 = p_k\left(1 - 2v^1\right) \approx \sigma_k$ – effective contact (critical) pressing pressure, calculated by Poisson's contact ratio v'; $p_к = p/\alpha$ – critical (contact) pressing pressure;

α – dimensionless active part of the volume of a porous body in which directed stresses or processes are concentrated;

v', v_k – Poisson's ratio (contact) of a porous and compact body.

The formula is of some interest [34]:

$$p = \frac{\sigma_S C \rho_{depend} \ln \rho_{depend}}{1 - \rho_{depend}}, \tag{2.11}$$

where σ_s – yield point of metal powder;

C – constant;

ρ_{depend} – relative density.

It is based on a comparison of the process of filling pores with the process of pressing through conical matrices.

However, this formula, like the formulas (2.9), is confirmed in practice in a relatively narrow range of pressures. In particular, compaction of electrolytic titanium powder in the pressure range of 196…696 MPa is described with acceptable accuracy by the previous dependence, which in this case will turn into the form:

$$\rho = \frac{3\rho_{depend} \ln \rho_{depend}}{1 - \rho_{depend}}. \quad (2.12)$$

A number of empirical dependencies of other studies [35] to one degree or another correspond to the given equations (2.9). The main drawback of the available compaction formulas is that the physical nature of the considered process is practically not taken into account, which is partly explained by the author's desire to obtain simple mathematical dependencies.

In order to give the formula a physical meaning, it is necessary to take into account the main factors affecting the process of compaction of metal powder: elasticity, plasticity, strength, friction parameters, scale factor.

Worthy of attention are the proposals considered in [36], which consist in rationally decomposing the compaction process into relatively independent elementary processes followed by their mathematical description. From this point of view, the monograph [37] is of interest, which shows the deformation mechanism of compaction of powder bodies, which includes elastic, plastic, structural and interparticle components of deformation (the structural component is a distinctive feature of the deformation of bulk bodies). The final equation of pressing in rigid matrices has the form [37]:

$$\rho 0 = \frac{p_k \left(1 + \frac{1}{2A_\beta}\right)\left(\beta_0^n - \beta^n\right)}{\beta^n \left(\beta_0^n - 1\right)}, \quad (2.13)$$

where p_k – yield pressure of the maximally hardened material;

$$A_\beta = \frac{\varepsilon \cdot f\left(L_H + L_B\right)h_k}{S_H}, \quad (2.14)$$

where ε – side pressure coefficient;

L_H, L_B – the values of the lengths of the perimeters or contours, respectively, of the outer and inner side surfaces of the pressing;

S_H – cross-sectional area of pressing;

h_k – critical or reduced pressing height at 100 % density;

β^n – relative pressing volume;

$\beta_0 = 1/V_0$ – initial values of the relative volume;

V_0 – relative bulk density.

However, the results of the calculation according to the specified formulas are slightly different from each other, since the same reasons are mainly used when deriving them.

An attempt to give a scientifically based relationship between the density of pressings (briquettes) and pressing pressure was made by L. A. Shofman, where the sliding line method, developed in detail in the theory of plasticity, was used to analyze the pressing process. **Fig. 2.5** shows the deformation model of compaction, in which the shape of the powder particles is taken as round cylinders.

As a result, an equation was obtained for determining the average pressing pressure, taking into account strengthening and frictional forces on the surface of the mold:

$$p = \frac{a}{1-\exp(-a)} A\sigma_B \left(1-0,4\beta_{cp}\right)^k \left[\frac{\lg 1}{\beta_{cp}-1}\right] - 0,4\left(1-\sqrt{\beta_{cp}-1}\right), \quad (2.15)$$

where $a = 4\mu H / D\beta_{cp}$ – for pressing a briquette of cylindrical shape by one-sided pressure; $a = 2\mu H / D\beta_{cp}$ – in the case of two-sided load application;

μ – coefficient of external friction;

$A = 2 / (1 - \psi_ш)\,\psi_ш^{\kappa}$;

$\sigma_в$ – strength limit; $\sigma_в = [\sigma_в/(1-\psi_ш)](\psi/\psi_ш)^{\kappa}$;

$\psi_ш$ – relative reduction of the cross-section of the tensile sample at the time of the beginning of neck formation;

ψ – level of deformation;

$\beta_{cp} = \rho_м \rho_{сер}$ ($\rho_м$ – density of non-porous metal; ρ_{cp} – average volumetric mass of pressing).

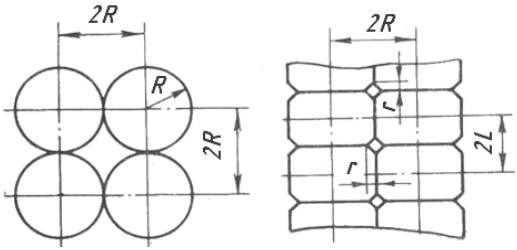

a *b*

a – before deformation; b – after deformation

Fig 2.5. Scheme of packaging of powder particles

The equations provide a satisfactory similarity with the results of experiments by a number of authors and are consistent with the known dependencies of the compaction process. However, the accepted model of pressing is rather abstract and therefore does not reflect the true picture of compaction.

For the practice of pressing, the experimental study of the compaction process is of great importance. **Fig. 2.6** and **Fig. 2.7** show the results of the study of the compaction process of titanium powders with aluminum. The degree of compaction at the same pressure depends on the method of obtaining the powder.

As the *H/D* ratio increases at the same pressing pressure, the density of the briquettes decreases. Analyzing the pressing process of powder made by the same method, but of a different fraction, it can be seen that the powder with fewer impurities and less hardness (large powder fraction) has a greater density at the same pressing pressure. With the traditional method of powder metallurgy, cold pressing followed by sintering, it is impossible to obtain non-porous structural products, the demand for which is growing. In addition, it is difficult to manufacture products of complex shape with minimal assumptions for further mechanical processing. All this led to the development of more effective methods of processing powdered metals.

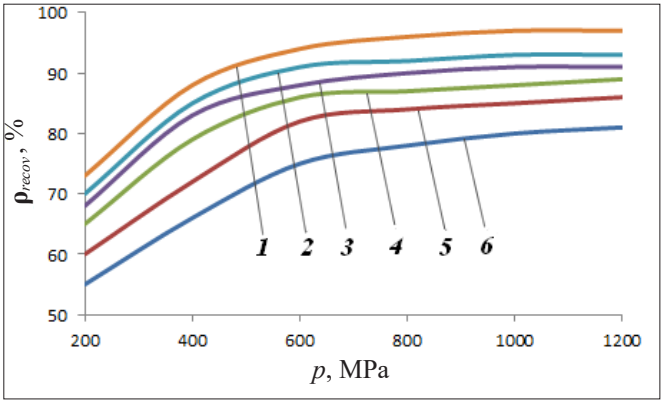

1 – H/D = 0,25; 2 – H/D = 1; 3 – H/D = 1,5; 4 – H/D = 2; (electric powder); 5 – H/D = 1 (calcium hydride powder); 6 – H/D = 1 (hydride powder)

Fig. 2.6. Dependence of the relative density of briquettes ρ_{recov} from pressing pressure *p* with different *H/D*

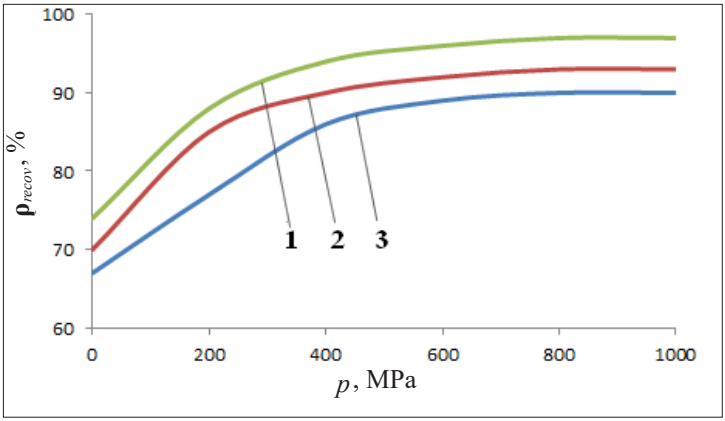

1 – (–1) + 0,5 mm; 2 – 0,5 + 0,18 mm; 3 – (–0), 18 + 0,08 mm

Fig 2.7. Dependencies of the relative density of briquettes ρ_{recov} from pressing pressure *p* of the electrolytic powder fractions

2.4. Hot deformation of synthesis products

When carrying out the second stage, the briquette was placed in a reaction mold – a matrix for hot pressing (Fig. 2.3, *a*) with a heat insulator, which can be either lining heat-insulating material or ordinary sand.

Combustion of the batch briquette is initiated in the mode of thermal self-ignition. Initiation of the reaction was carried out by preheating to the temperature of the beginning of spontaneous ignition. The time of passage of the combustion wave through the batch billet corresponds to the time of synthesis (reaction) $t_r = 0.5…15$ s. After the end of combustion, after a certain delay time of pressing (1…5 s), necessary for the removal of the gases formed, additional pressing (compaction) and exposure of the sample under this pressure begins. The exposure time is determined by the compaction time $t_k = 3…120$ s. During the next 20 minutes, the reactor was allowed to cool, after which the synthesized material was discharged from the matrix.

The required volume of the workpiece, taking into account the final porosity of the pressed products, is determined by the expression:

$$V_3 = V_c \frac{(\rho_c - \Pi)}{\rho_б}, \qquad (2.16)$$

where V_c – volume of the cast metal workpiece;

ρ_c, ρ_b – relative density of cast metal and cold-pressed blanks;

Π – residual porosity after hot pressing.

Before pressing, the blanks are heated in electric resistance furnaces with a controlled atmosphere or in induction heaters. The heating medium is selected depending on the activity of the alloy base: for titanium blanks, an inert medium is argon. The temperature range of pressing for a titanium powder billet is 950…1000 °C. In the initial period of heating, due to low values of thermal conductivity, large temperature differences are possible across the cross-section

of the workpiece, which leads to the appearance of thermal stresses, as a result of which the heating of titanium powder workpieces in resistance furnaces must be carried out with endurance at the pressing temperature. During induction heating, heat is generated directly in the body of the workpiece itself under the action of eddy currents induced in it, so induction heating of workpieces can be produced at a higher speed than heating in resistance furnaces. The study of the power regime of hot pressing of powdered titanium is shown in **Fig. 2.8.**

It was established that the nature of the change in pressing force in both open and closed dies reveals a general regularity that does not depend on the ratio of the diameter of the workpiece to the height *D*/*H*, and is described by a curve close to a parabola of the 4th degree.

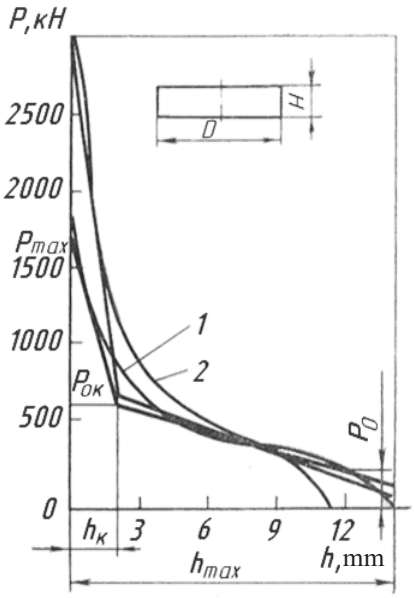

1 – opened stamp; 2 – closed stamp

Fig. 2.8. Loading graphs of pressing

The mechanical diagram of the deformation of the powder blank in the closed die is shown in **Fig. 2.9**, *a*. At the initial moment of deformation, there is an uneven all-round compression of the workpiece with insignificant lateral compressive stresses, which increase as the die cavity is filled and reach significant values by the time the metal flows into the compensators and the die cavity is finally filled. Uniform all-round compression takes place, which is very important for obtaining a product with uniform density throughout the entire volume.

The mechanical diagram of the deformation of the powder blank in the open die at the final stage is shown in Fig. 2.9*, b*. In this case, there is also a comprehensive compression, but the magnitude of the compressive lateral stress is much smaller than the main axial stress. This scheme is less favorable compared to pressing in a closed die and is characterized by a large uneven deformation, which leads to deterioration of the microstructure and mechanical properties of the products. The difference in the power mode of hot pressing of the powder blank in open and closed dies is observed only in the final stage of pressing. A significant increase

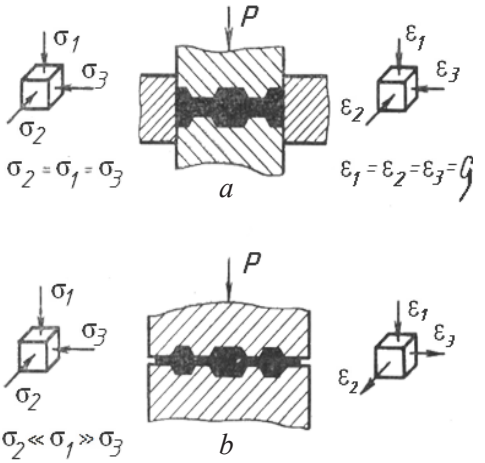

Fig. 2.9. Mechanical scheme of deformation in closed (*a*) and open (*b*) stamps

in specific forces in the closed stamp at the end of pressing is due to the comprehensive compression of the workpiece in the closed cavity of the stamp and only a small end of it in the compensators. In an open die, excess metal flows out along the entire perimeter of the part at much lower compressive stresses. The calculation graph can be approximated by two straight lines. Having drawn tangents to the curves in the corresponding sections, we denote the ordinate of the point of intersection of the tangents $P_{o.к}$, the abscissa $h_к$, the largest working stroke h_{max}, the force corresponding to the beginning of the working stroke, P_0, the maximum force P_{max}. The ratio P_0/P_{max}, $P_{o.к}/P_{max}$, h_{max}/R (where R is the radius of the crank) fully characterizes the force mode of pressing on crank presses (**Table 2.4**).

Table 2.4. Power mode of pressing on crank presses

Stamp	H/D	h_{max}/R	$h_к/R$	P_0/P_{max}	$P_к/P_{max}$
Open	1.1	0.28	0.014	0.03–0.05	0.21
	0.3	0.05	0.013	0.03	0.39
Close	1.1	0.29	0.021	0.014	0.127
	0.3	0.05	0.12	0.02	0.26

To date, uniform calculation formulas have not been obtained for determining the force mode of pressing in closed dies.

The complexity of the process of metal flow in a closed die complicates the conclusion of such formulas for calculating pressing forces. The pressing process must be considered in the last stage of deformation, when the metal flows into the compensating gaps, and the force will be maximum.

The following expressions can be used to determine the pressing force of parts that are round in plan [39]:

$$P = p\omega\sigma_s F_n, \tag{2.17}$$

where ω – temperature–velocity coefficient;

σ_s – yield strength at deformation temperature;

F_n – forging area in plan;

p – average pressure at the time of leakage.

$$p = 2,3 + 1,35 \ln \frac{D_n H_{cp}}{a \cdot l} - \left(\frac{1,2\sqrt{\frac{a \cdot l}{\pi}}}{D_n} + 0,7 \right) \ln z + \quad , \quad (2.18)$$

$$+\mu \frac{D_n}{H_{cp}} \left(1,2 - 0,2z \sin \frac{180^o}{z} \right) + 4\mu \frac{H_{cp} - \frac{a}{2}}{D_n},$$

where μ – coefficient of friction;

D_n – diameter of the forging;

$H_{cp}=V_{пок}/F_{пок}$ – the average height of the forging;

a, l – height and width of the compensation window;

z – number of windows.

The peculiarity of the process of hot pressing of blanks from titanium powders (**Fig. 2.10**) is that the main shape change of the metal occurs at the early stage of deformation, when the forces are small.

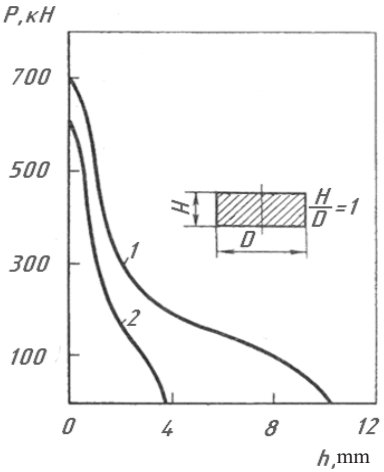

1 – cast billet; 2 – powder billet

Fig. 2.10. Loading graphs of pressing

In the final stage, metal pressing is insignificant, as it is mainly compacted and the final deformation of the forging takes place.

This is due to the fact that the powder blank can be obtained in a form close to the product.

In the process of pressing parts from powder blanks, there is no intense fluidity of the metal, and therefore, increased wear of the tool at the time of application of maximum working effort.

The advantages of this process also include the absence of a burr, the formation of which is associated with a sharp jump in the amount of work effort with a corresponding increase in the final stage of the formation of local wear of the tool.

Foil-free pressing is one of the progressive high-performance methods of processing metals by pressure, however, intensive wear of the tool leads to a significant spread in the dimensions of stamping. To obtain dimensionally stable pressed products, it is necessary to reduce wear to a minimum, which is associated with the need to significantly reduce the loads acting on the tool. In this regard, the process of coating-free pressing of blanks from metal powders is promising.

The nature of compaction of powder materials in the process of deformation has much in common with ordinary slander. The areas of the pressed briquette-preparation, first of all, come into contact with the tool, are accordingly compacted and in the future provide increased resistance to deformation.

When overcoming the frictional forces, the compacted volumes can again be involved in the flow of metal during deformation. “Hard zones” correspond to zones of reduced density, which refer to serious defects in powder forgings.

The porosity of the initial blank does not significantly affect the density of the final product. The use of powder blanks with a higher density is advisable from the point of view of reducing the active surface of oxidation during heating before pressing, however, in this case, it is worth paying attention to the uniform distribution of density

throughout the volume of the billet and to the value of cold pressing pressure, the increase of which leads to significant wear tool and more energy consumption.

Preliminary sintering of blanks of a simple shape does not significantly affect the process of shape change and energy modes of pressing (**Fig. 2.11**). For parts with a complex shape, different from the shape of the final product, preliminary sintering is advisable, as it prevents the appearance of cracks during pressing.

The pressing of complex alloyed powders in order to ensure the most complete homogenization of the alloy is advisable to be carried out in isothermal conditions, in which, along with the simplification of further heat treatment, there is no need for preliminary sintering of the blanks.

When pressing forgings from powdered cylindrical blanks due to cracking of the briquette during settling, it is possible to lock oxidizing

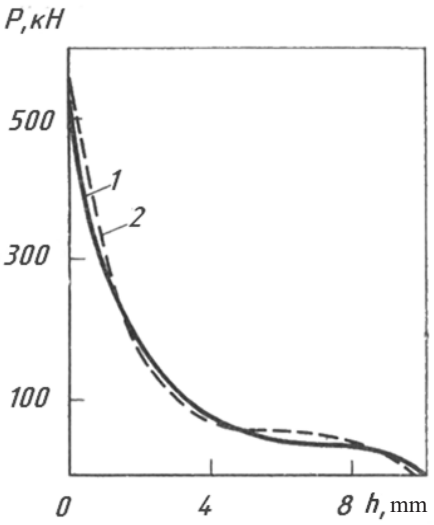

1 – workpiece without prior sintering; 2 – workpiece, pre-baked

Fig. 2.11. Loading schedule of pressing

areas and infiltration of lubricant into the product, which can be traced at the first stage of pressing. Therefore, it is advisable to bring the shape of the workpiece closer to the shape of the stamp engraving.

Compaction of the powder mixture occurs due to the reduction of the volume of air inclusions in the material and the closing of macropores. This is due to the compressibility properties of the powder material.

The density of the sample also plays an important role in the possibility of the thermal self-ignition mode. The volume thermal explosion mode is observed only for samples with a high density of 55…70 %.

During pressing, there is a decrease in grains with a simultaneous increase in their total surface area. This is facilitated by the intensification of intergranular diffusion, which proceeds at a significantly increased speed due to high specific force and temperature.

Intense plastic deformation of particles contributes to the formation of oxide-free contact surfaces, activates direct interaction between particles, thereby increasing the number of metallic bonds, which is confirmed by metallographic studies and measurement of specific electrical resistance. The study of the microstructure of the obtained products based on powdered titanium shows that during hot pressing a high density is achieved over the entire cross-section of the product. As a result of rapid cooling, the surface layer has a finer grain compared to the larger grains inside the product, which are somewhat oriented towards deformation. Further heat treatment (annealing) relieves the internal stresses of hot pressing, resulting in the formation of an equilibrium polyhedral structure of the α-phase.

The pressing density reaches 98…99 % of the theoretical one, which meets the requirements for heavily loaded parts. The residual porosity of intermetallics is 1…3 %.